Star Tracker Performance Estimate with IMU

Eliot Aretskin-Hariton* and Aaron J. Swank†
NASA Glenn Research Center, Cleveland, OH, 44135

A software tool for estimating cross-boresight error of a star tracker combined with an inertial measurement unit (IMU) was developed to support trade studies for the Integrated Radio and Optical Communication project (iROC) at the National Aeronautics and Space Administration Glenn Research Center. Typical laser communication systems, such as the Lunar Laser Communication Demonstration (LLCD) and the Laser Communication Relay Demonstration (LCRD), use a beacon to locate ground stations. iROC is investigating the use of beaconless precision laser pointing to enable laser communication at Mars orbits and beyond. Precision attitude knowledge is essential to the iROC mission to enable high-speed steering of the optical link. The preliminary concept to achieve this precision attitude knowledge is to use star trackers combined with an IMU. The Star Tracker Accuracy (STAcc) software was developed to rapidly assess the capabilities of star tracker and IMU configurations. STAcc determines the overall cross-boresight error of a star tracker with an IMU given the characteristic parameters: quantum efficiency, aperture, apparent star magnitude, exposure time, field of view, photon spread, detector pixels, spacecraft slew rate, maximum stars used for quaternion estimation, and IMU angular random walk. This paper discusses the supporting theory used to construct STAcc, verification of the program and sample results.

Nomenclature

μ	population mean
ω_d	slew rate in degrees per second
ω_p	smear in pixels
σ	population standard deviation
σ^2	population variance
σ_C	standard deviation of the centroid
σ_P	standard deviation of photons from a star as seen by the star tracker
σ_{imu}	angular random walk of the IMU
a	aperture
d_p	pixel width of the detector
E_R	Roll Error
E_{XB}	Cross-Boresight Error
m_V	apparent star magnitude
n	sample size
N_{star}	number of stars that the star tracker is observing
s^2	sample variance
t	exposure time

I. Introduction

THE Integrated Radio and Optical Communication (iROC) project is a research and development effort to couple deep space radio frequency and optical communication elements into an integrated system. Free

*Ast Control Engineer, Intelligent Control and Autonomy, 21000 Brookpark Road, Cleveland, Ohio
†Research Engineer, Information and Signal Processing, 21000 Brookpark Road, Cleveland, Ohio

space optical communication is of interest to the National Aeronautics and Space Administration (NASA) as an alternative to radio frequency communication. Optical communications systems, as compared to traditional radio frequency communication methods, promise a substantial increase in data return with a corresponding savings in mass, power and volume requirements. With a comparable communications subsystem mass to that of the Mars Reconnaissance Orbiter (MRO), the iROC payload has the potential of exceeding 26 times the data downlink rate using only optical communication.[1] Considering that a single High Resolution Imaging Science Experiment (HiRISE) image from the MRO takes over 1.5 hours to be transmitted from Mars to Earth, a shift to optical communication would result in a substantial increase in the received mission data.

Although optical communication promises a number of substantial improvements over state-of-practice radio frequency communication, free space optical communication is not absent of technological challenges. Radio communication is transmitted in a broad beam illuminating a target area, whereas optical communication utilizes a comparatively narrow beam, pointed at a single receiver. While the narrow optical beam results in more efficient use of the electromagnetic spectrum, free space optical communication is challenged by more stringent pointing and tracking requirements due to optical beam divergence. Historical methods for free space optical communication rely on closed-loop tracking of an Earth-based communication beacon. The Lunar Laser Communication Demonstration (LLCD) has shown that a beacon-aided laser communications technique is feasible for near earth orbiting satellites.[2] Yet for deep space optical communication from Mars or beyond, beacon-aided optical communication is less practical.[1] Thus, alternatives to beacon-based laser communications are being investigated for the iROC project.

The iROC project is evaluating the use of star trackers combined with a high-rate inertial measurement unit (IMU) for precision attitude determination. Precision attitude information, combined with satellite state information, eliminates the need for a ground-based beacon, which increases spacecraft autonomy and enables laser communications at Mars and into the far reaches of the solar system. For establishing beaconless optical communication from Mars to Earth, the iROC design requires an optical beam pointing accuracy on the order of 2 to 5 μrad. Selecting the combination of attitude determination hardware within reasonable mass and power constraints is a challenge to produce the necessary precision attitude information for autonomous beaconless optical communication.

The Star Tracker Accuracy (STAcc) tool presented in this work creates a foundation for analyzing attitude knowledge based on expected star tracker and IMU performance information. This paper first introduces previous methods of star tracker characterization including those by Liebe[3] and Dzamba.[4] Methods to expand the preexisting models based on additional needs of the iROC project are then covered. Finally, the completed method, as embodied by the STAcc tool, is presented and a verification of the tool is conducted.

II. Methodology and Development

Models describing the accuracy of star trackers are essential for building an understanding of how individual star tracker physical parameters affect the overall star tracker accuracy metric. While these models do not substitute for hardware testing of the star tracker, they do provide a low-cost alternative that allows multiple design configurations to be evaluated without the need to purchase hardware. The use of accurate models is a valuable design assistance tool in the preliminary phases of a project. For example, the iROC project is currently in the pre-formulation phase and initial analyses indicate that the required attitude information is near the limit of current star tracker performance capabilities. By using software models which estimate the star tracker performance as a function of star tracker physical parameters, one can estimate or predict what capabilities may exist in the future given current advancements in sensor technology. For example, currently under development is the High Accuracy Star Tracker 3 image sensor (HAS3), a next generation complementary metal-oxide-semiconductor (CMOS) image sensor, intended to replace the commonly used HAS2 sensor. By using the manufacturer estimated performance characteristics of the next generation image sensor, one can use the models to estimate the performance of the next generation star tracker hardware using the sensor.

In order to describe the methodology developed and used in this work, first a review of prior work will be presented. The overview of prior published work will be followed by a new method, which expands on the prior work, to include effects of non-zero rotation rates and IMU coupling. The results from this analysis are incorporated into the STAcc program which is used to estimate capabilities of star tracker and IMU systems.

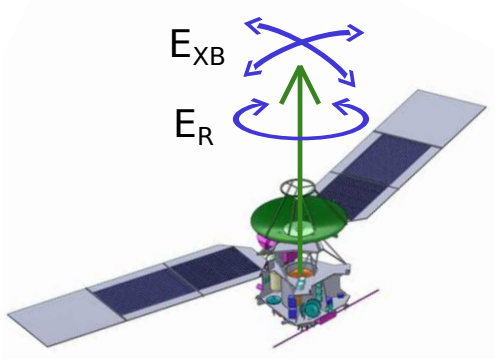

Figure 1. Cross-Boresight Error vs. Roll Error. The star tracker is mounted along the green arrow.

II.A. Previous Work

Work to characterize star tracker accuracy and performance has been conducted by Liebe[3] and Dzamba.[4] The model presented here is based on equations as presented by Liebe, which contain a method for estimating cross-boresight error (E_{XB}) and roll error (E_R). A visual representation of E_{XB} and E_R can be seen in Figure 1. Liebe's model predicts performance based on the following parameters: quantum efficiency (QE), aperture (a), apparent star magnitude (m_V), exposure time (t), field of view (FOV), detector pixels (d_p), the number of detected stars that the star tracker can see (N_{star}), and standard deviation from the photon source (σ_P).

$$E_{XB} = f(\text{QE}, a, m_V, t, \text{FOV}, d_p, N_{star}, \sigma_P), \tag{1}$$

The last term is equivalent to the standard deviation of the photon Gaussian distribution that describes the distribution of photons incident on the detector. Liebe refers to σ_P as the Point Spread Function (PSF) radius. In the work of Liebe, a quantum efficiency of 100% and a 9×9 pixel window are assumed. This means that all photons are converted to electrons by the detector. These results are easily scalable to lower quantum efficiency levels. Yet, in the work of Liebe, the results which are based on the 9×9 pixel window assumption, are not easily scaled. In addition, Liebe's work assumes a detector slew rate of zero. In this paper, a slew rate or rotation rate of zero means that the star tracker is not rotating with respect to the inertial frame. In this case, stars appear as crisp points of light as opposed to smears. The zero slew rate assumption for star tracker performance estimation is the motivation for the work performed by Dzamba et al.[4] Dzamba extended Liebe's work to rotating spacecraft, by modeling star tracker performance for high slew rate applications, specifically for micro satellites. The Dzamba model also contains multiple other inputs to quantify additional error sources such as shot noise, saturation, electron quantization and photon signal to noise ratio. Dzamba's approach to modeling the centroid smear due to high slew rates is to derive an equation that describes the new smeared distribution used to model the star light. As a spacecraft rotates or slews in space, the centroid of the stars appear to smear across the surface of the detector, which introduces additional errors into the centroiding process (Figure 2). Typically a point spread or a Gaussian function is used to model the light emitted by a star. However, the actual observed distribution is altered by the slew rate. How the distribution is altered depends on many factors including the physical hardware makeup of the star tracker as well as the slew rate. The resulting distribution is hardware specific and as such, it represents a point design approach where the Monte Carlo analysis must be run once per hardware configuration.

In contrast to Dzamba, the approach taken in this paper is to model the effects of smear using a non-hardware specific approach. This enables the Monte Carlo analysis to be conducted without specifying the hardware configuration of the star tracker. In addition, the approach presented here is not limited to the zero rotational rate assumption and is applicable to pixel windows of other sizes. The presented method is further extended to incorporate an IMU with the star tracker measurements. As such, this effort explores extending the work presented by Liebe to incorporate slew rate and IMU accuracy as parameters in the performance analysis.

(a) Still image of star (b) Smeared image of star

Figure 2. Comparison of detected star light from still vs. rotating camera.

II.B. Centroid without Rotation

Integral to Liebe's analyses are sub-pixel accuracy lookup tables (Figure 4 as discussed later). Sub-pixel accuracy (σ_C) refers to the 1σ confidence interval (CI) at which the individual star centroid locations are determined and is a key determinant of the overall star tracker error. Liebe's lookup tables allow one to determine the expected σ_C as a function of the number of electrons captured by array (n) and the spread of the light through the aperture (σ_P).

$$\sigma_C = f(\sigma_P, n), \tag{2}$$

Using a lookup table is efficient for large photon counts where running a thorough, on-demand Monte Carlo simulation is numerically intensive. In order to alter Liebe's lookup tables to include non-zero slew rates, a third characteristic is added to the lookup table corresponding to the number of pixels over which the star's light is smeared. Using this factor, one avoids a hardware specific solution while constructing the sub-pixel error lookup tables. In addition, methods to determine lookup tables for both sub-pixel jitter and bias error must be applied. Once the lookup tables are created, one can then correlate the number of pixels over which the light is smeared for a given rotational rate. This is covered in the next subsection.

To create the new lookup tables of sub-pixel accuracy, a Monte Carlo analysis is designed to simulate photons hitting a detector. The simulated detector is represented by a pixel array, which is 9×1 pixels in extent. Simulated photons striking the detector are binned onto individual detector pixels. The detector is assumed to exhibit a 100% QE and fill factor, which allows for the resulting tables to be scaled for realistic electron conversion efficiencies. The location of the photon population mean (μ), which corresponds with the true center of the star on the detector, is placed at the center of the detector. A Gaussian distribution is used to describe the effects of photons emitted from a star when the spacecraft exhibits near zero rotational body rates. The photon spread value (σ_P) is used as the population standard deviation for the Gaussian distribution. Photons are created until the specified sample size n (number of electron counts) has been reached. Finally, centroiding is performed on the illuminated pixels using a center of mass method.

Many different types of noise affect star tracker performance. It is important to note that the effects from shot noise, read noise, stray light, or other noise effects are not included in this simulation. An initial analysis of the effects of not including noise is presented at the end of this section. In Liebe's analysis, some limited noise effects were included. Yet, Liebe's lookup tables only contain error due to jitter and cannot be used to determine bias error. As noted by Jia et al.,[5] the offset or bias error is affected by the location of the photon population mean, (μ). When the population mean is located at the center of the pixel, the bias error is small. For detectors where the ratio of detector width to σ_P is large, bias error is also small. Bias error appears at a maximum when μ is located half way between the center and the edge of a pixel. The relationship between offset error as a function of centroid location and σ_P is graphically depicted in Figure 3. In Figure 3(a), maximum offset corresponds to the case where μ is located half way between the center and the pixel edge. In comparison, for small detectors with large photon spread relative to the pixel size, Figure 3(b), the highest bias error occurs at the edges between pixels. Error is minimized by setting photon spread to be between 0.4 and 0.6 pixels (Figure 3(b)). Thus, regardless of the location of μ, the least amount of bias error is introduced. The optimum σ_P may vary as a function of detector size. In hardware, σ_P is modified by changing the shape of the lens of the star tracker. The STAcc model assesses the cross-boresight error from three blocked groups, where μ is varied from the pixel center, to a 1/4 pixel offset and finally to the pixel edge. To be conservative and to remove pixel offset as an input parameter, only

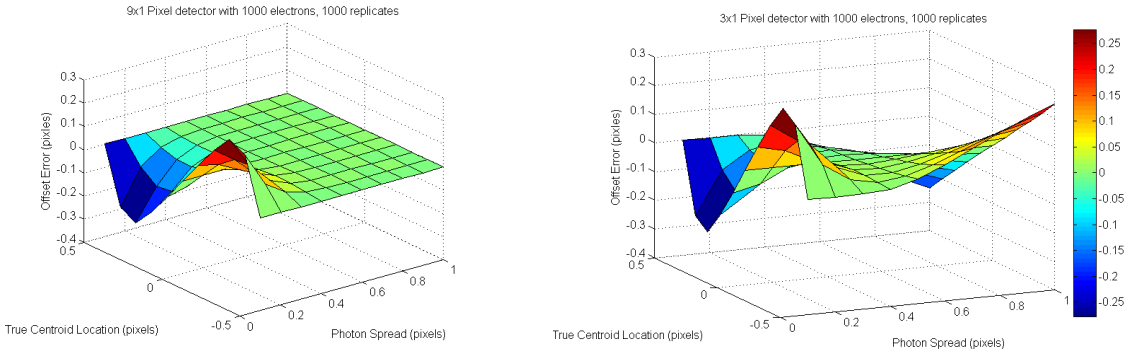

(a) 9×1 Pixel Detector

(b) 3×1 Pixel Detector

Figure 3. Cross-boresight offset error effects due to photon spread (σ_P), and photon source location (μ), is shown to be consistent with Jia et al.[5]

the largest error from these three groups is used in the lookup tables. As a result, errors from the location of μ are included in a conservative manner.

For the simulation and table generation, the true centroid position μ, photon spread σ_P, electron count n, and slew rate are varied for the simulation. The value of μ is varied from 0.5 pixels offset from the center to the detector center in increments of 0.25 pixels. The value of σ_P is varied from 0.5 to 2.0 pixels in increments of 0.5 pixels. Electron counts are varied on a logarithmic scale from 10E3 to 10E6 in powers of 10. To determine the sample variance (s^2) of the centroiding for each blocked group, 1,000 replicates of the experiment are conducted. In so doing, the pixel width and windowing errors are included into the variance term. The confidence interval on the sample variance is small when 1,000 replicates are used. Thus, it is reasonable to assume that the sample variance (s^2) is similar to the population variance (σ^2). A translation from 1-D to 2-D is made by summing twice the variance of the 1-D model and taking the square root. The population standard deviation is then used as the sub-pixel jitter error for the lookup table. The bias lookup tables are obtained by taking the absolute value of the difference between the sample grand mean and the true mean. The final tables contains the worst case true centroid position offset and jitter erros. The worst case is calculated by taking only the largest value for both jitter and bias error from the three sample groups. The generated jitter lookup tables are used as a substitute for that presented by Liebe, and allows one to determine cross-boresight jitter in micro-radians. An illustrative example comparing the lookup tables as published by Liebe[3] to that of this work is shown in Figure 4.

In both graphs from Figure 4, accuracy decreases as electron counts increase. This is expected because centroiding algorithms are more accurate as more samples are taken. For a star tracker, a smaller sub-pixel accuracy is desired and σ_P is chosen to ensure this. There are some noticeable differences between Liebe's table (Figure 4(a)), and those created by this work (Figure 4(b)). Liebe's work shows larger accuracy for σ_P of 2.0 and 2.5 pixels. This is expected because that analysis included noise sources. Noise has a larger effect when the incoming light is spread over a larger number of pixels. However, sub-pixel accuracy is minimized by choosing a smaller σ_P. For σ_P values of 0.5, 1.0, and 1.5, Figure 4(b) has larger accuracy. The values in Figure 4(b) were calculated without including noise effects. This means that for small σ_P, a worst-case estimate of sub-pixel accuracy is obtained by using the table from Figure 4(b), even though the table was created without noise effects. These differences may be attributed to methods of centroiding or study design.

II.C. Centroid with Rotation

The process to generate sub-pixel accuracy lookup tables is readily adapted to the case with non-zero rotational rates. For a non-zero rotational rate, an additional factor is added to the lookup table generation process which captures the smear in pixels across the detector. As an illustrative example of how slew rate relates to image smear, consider the case of a pinhole camera as shown in Figure 5. The rotation of the camera detector with respect to the star source results in image smear across the detector. Smear of the star image causes the nominally symmetrical photon distribution σ_P to elongate across the detector surface. The new σ_P across the detector results in a larger illuminated portion of the detector surface. A non-zero slew rate creates a varying amount of image smear on the detector array, depending on the selected camera

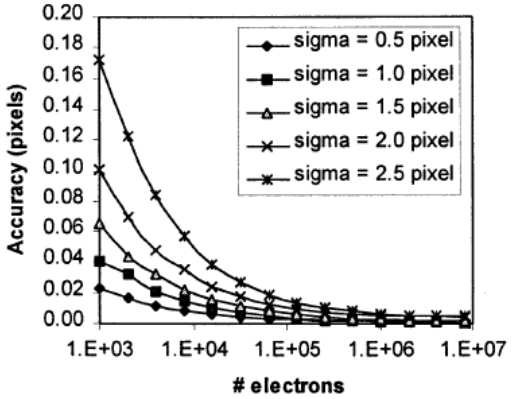

(a) Sub-pixel accuracy as presented by Liebe.[3] Slew rate is always 0°/s.

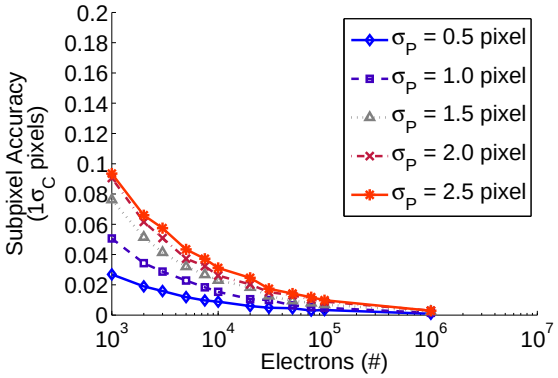

(b) New sub-pixel accuracy lookup tables, which include slew rate. Slew rate is set to 0°/s for comparison.

Figure 4. Centroid sub-pixel accuracy as a function of photo electron count and photon spread.

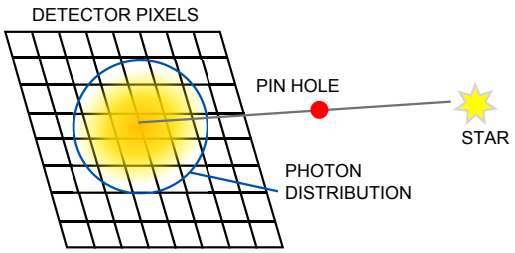

(a) Nominal, zero slew rate condition.

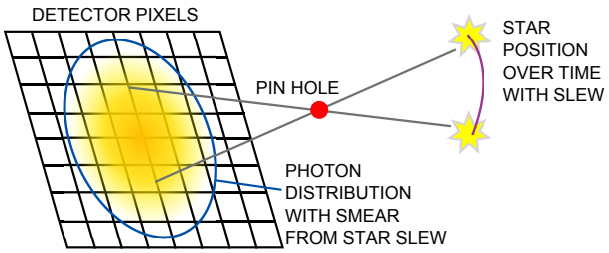

(b) Star light smeared by camera rotation and resulting smear on the detector array, non-negative slew rate.

Figure 5. Illustrative comparison of star light mapped to pixel detector for zero and non-zero slew rates.

hardware. Multiple hardware options may exhibit the same smear length despite having different hardware design parameters. Thus instead of specifying a slew rate for the lookup table factor, the smear in pixels is specified. For this analysis, it is assumed that the change in star position on the detector due to non-zero slew rate is small relative to the total detector size. Skewing effects on the detector due to large angle rotations may therefore be ignored.

In order to create the new σ_P, which is observed due to slew effects, an alternative approach is taken to the hardware specific approach presented in Dzamba.[4] Here, the Monte Carlo analysis is modified to create photons by coupling a uniform distribution with a Gaussian distribution. By combining the two distributions, the effect of a star moving across the detector during the exposure time is simulated. The Gaussian distribution describes the nominal photon distribution for zero slew rates, while the uniform distribution is used to describe the location of the star as it moves across the surface of the detector. Here it is assumed that a star moves uniformly across the detector during the exposure period and does not dwell or spend disproportionate time at a specific location. In order to accommodate the new smeared image, the equivalent detector size must be increased. Originally, a 9×1 pixel box was used for the non-slewed configuration. For the slewed case, the detector array is increased by 120 pixels to create a 129×1 pixel array. Expanding the array by 120 pixels was chosen to allow typical star trackers to slew up to 5 degrees per second. The exact amount of pixel smear will depend on both the slew rate and the star tracker hardware.

To get a preliminary understanding of how slew could affect the centroiding results, a Monte Carlo analysis is conducted. In this preliminary analysis, the starting location for the star is set to 4.5 pixels and the end location is varied from 4.5 to 124.5 pixels. From the initial analysis shown in Figure 6, large variations are evident in cross-boresight offset error due to small changes in smear effects. Therefore an approach is taken where only 30 blocked groups around 120 pixels of smear is analyzed. Then the upper 99% (CI) of the combined results is used as the expected error. With a sample size of thirty, the central limit

theorem applies, and a 99% upper confidence interval for the value of the errors is constructed (Figure 6). The confidence intervals are saved in the table as the expected offset error from centroiding. Random errors are determined in a similar fashion. After the largest expected jitter and bias error for 120 pixels of smear is determined, the Monte Carlo analysis is used to construct the tables with slew effects included.

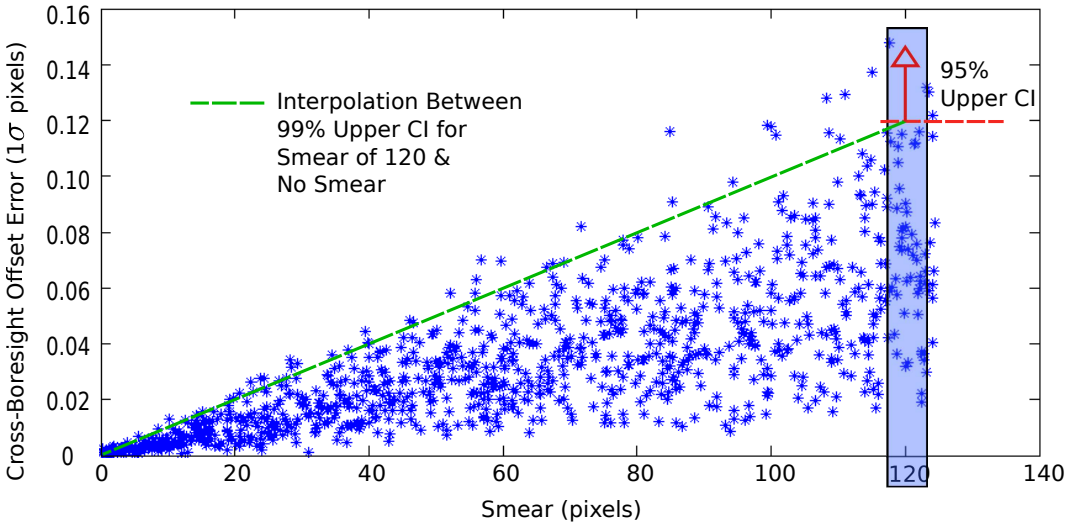

Figure 6. Smear distribution interpolation used for STAcc.

Once the tables for sub-pixel bias error are constructed for the cases which contain smear and do not contain smear, the tables can be combined to create a single 4-D lookup table. The resulting tables are substituted into Liebe's original analysis. The equations as presented by Liebe may be used directly with the modified look-up table results as the basis for determining cross-boresight jitter and cross-boresight offset error. The final look-up table takes as input parameters the electron count, σ_P, and number of smear pixels. Electron count is interpolated on a log-normal scale. σ_P and smear pixels are interpolated linearly. Similarly, the lookup tables for sub-pixel jitter error are combined and interpolated.

In the STAcc program, the hardware specifications and slew rate are used to derive pixels of smear, which is then used as an input for the look-up table. By using the pin hole camera model, the dependency between the change in the observed star pixel location due to a non-zero body frame rotational rate is easily obtained. The equivalent change of location in pixels for a given slew rate is given by:

$$\omega_p = \frac{\omega_d \; t \; d_p}{\text{FOV}}, \tag{3}$$

where ω_p is smear in pixels, ω_d is slew rate in degrees per second, t is exposure time in seconds, d_p is the detector size in pixels, and FOV is the field of view diameter in degrees.

II.D. IMU Coupling

Typically an attitude estimation system is comprised of an inertial rate sensor or IMU for high frequency rate information with periodic star tracker attitude measurement updates. The IMU performance characteristic is represented by the angular random walk (ARW) in degrees per square root hour. This characteristic represents how accurate the IMU is and a smaller ARW means less error from IMU measurements. Multiplying the ARW value by the square root of the exposure time yields the ARW per time step. From an initial star tracker measurement, the attitude error will grow quadratically over time as the IMU measurement is propagated. Refer to Figure 7 for an illustrative example of how the measurement error grows with time. In Figure 7, the standard deviation of a star's estimated location after a single star tracker reading is shown in dark blue at T_0. How the error grows over time until time T_1 is shown by the light blue dashed lines. The error from the reading at T_0 propagated to time T_1 is shown in light blue. A star tracker measurement is obtained at T_1 and the resulting error from the single measurement is shown in dark blue. Using a root sum of squares (RSS) approach, the errors of the T_0 and T_1 readings are combined. This method gives more weight to information with less error (smaller dark-blue circles in Figure 7). The resulting RSS error is shown

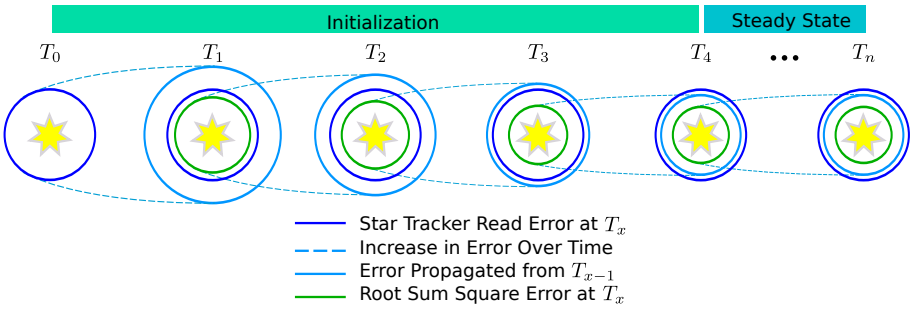

Figure 7. Estimated star location with error growing due to IMU propagation between star tracker updates.

in the green circle. This information is then propagated forward to T_2 (dashed blue lines). The process of taking star tracker measurements and combining them with IMU propagated data is a continuous process. The process generally goes through two phases. The first phase is an initialization phase during which the error is reduced rapidly. The second is a steady state phase, during which the error has a constant profile.

To combine multiple readings of a single star tracker, it is assumed that the cross-boresight error given by the star tracker is the same at each time step. This is equivalent to looking at the same set of stars at every time step, which is a reasonable assumption for small slew rates. Using rotational rate measurements from the IMU, information from prior time steps is propagated forward. In order to combine measurement error from multiple time steps, a least squares weighting is used. Further information is found in numerous texts, including for example, Borenstein et al.[6] Given the standard deviation of the star tracker, σ_o, at time t_o and σ_1 at time $t_1 = t_o + \Delta t$, the combined standard deviation, σ_{tot}, is calculated using the formula:

$$\sigma_{tot} = \sqrt{1/\left(\frac{1}{{\sigma_o}^2} + \frac{1}{{\sigma_1}^2}\right)} \tag{4}$$

The standard deviation (σ_1) at a Δt time later is described by the initial standard deviation (σ_o) plus the effects of the IMU random walk using the root sum square of the standard deviations. The equation for σ_1 is then given by:

$$\sigma_1 = \sqrt{{\sigma_o}^2 + \left(\sigma_{imu}\sqrt{\Delta t}\right)^2} \tag{5}$$

where σ_{imu} is the IMU random walk in radians per square-root second, and Δt is the number of seconds since the original observation. The standard deviation at any time is found by substituting Equation 5 into the expression for the total standard deviation, Equation 4, to yield:

$$\sigma_{tot} = \left(\frac{1}{{\sigma_o}^2} + \frac{1}{{\sigma_o}^2 + \left(\sigma_{imu}\sqrt{\Delta t}\right)^2}\right)^{-1/2} \tag{6}$$

Equation 6 provides an estimate for the error associated with using an inertial rate sensor and then propagating forward the solution with periodic star tracker updates as a function of time.

III. STAcc Description

THE methods described in Section II are used to create the Star Tracker Accuracy (STAcc) program. This includes: Monte Carlo simulations to create a table of sub-pixel jitter and bias error for no smear and 120 pixels smear, creating a 4 dimensional lookup table which allows interpolation between no smear and 120 pixels smear, photon spread (σ_P), electron counts, and sub-pixel jitter or bias error. These lookup tables are then used inside of the STAcc program along with the user specifications of star tracker and IMU hardware configuration to provide a quick estimate of system capabilities. The completed STAcc program allows the user to input 10 performance values of a star tracker and IMU system.

$$E_{XB} = f(\mathrm{QE}, a, m_V, t, \mathrm{FOV}, d_p, N_{star}, \sigma_P, \omega_d, \sigma_{imu}), \tag{7}$$

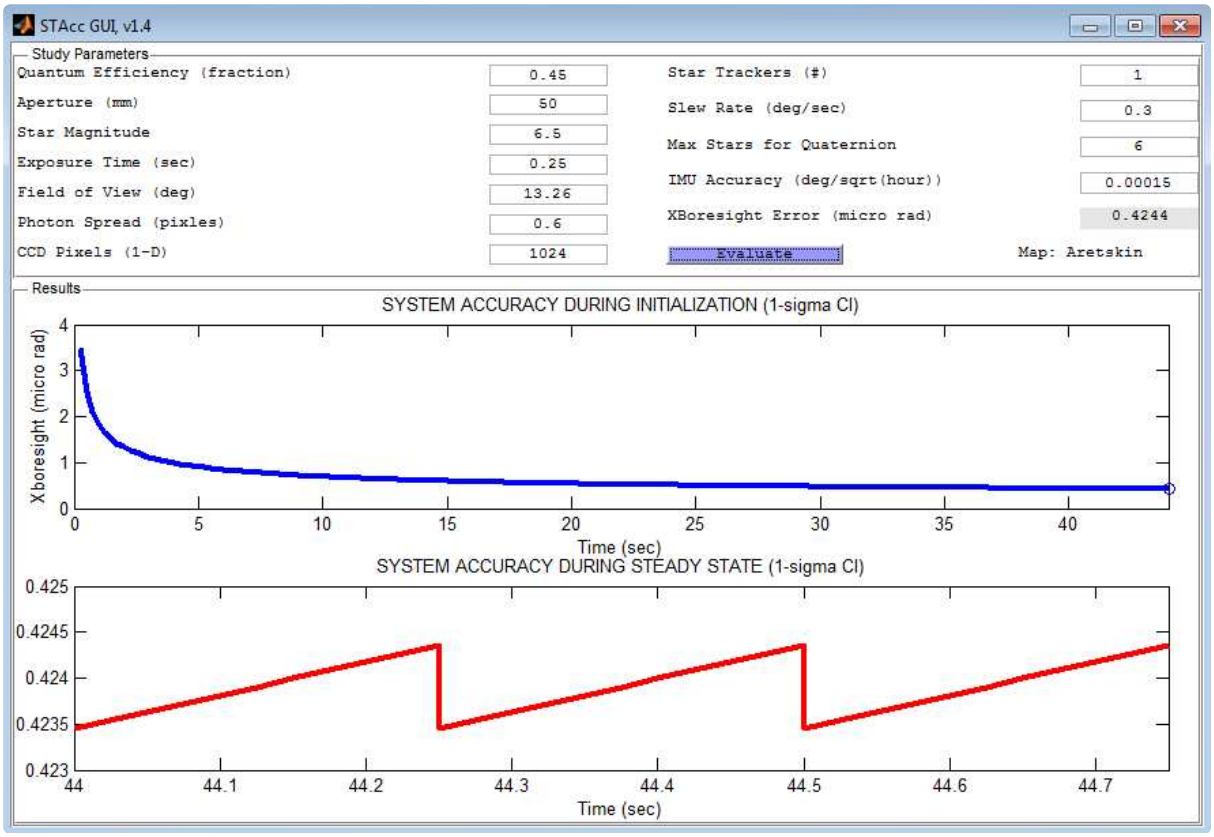

Figure 8. STAcc program interface and results for Astro 15 star tracker with IMU.

Where QE is the quantum efficiency of the detector, a is the aperture, m_V is apparent star magnitude, t is exposure time, FOV is the field of view, d_p is the width of pixels on the detector, N_{star} is the number of detected stars that the star tracker can observe, and σ_P is the standard deviation from the photon source. The two remaining terms are ω_d, which is the slew rate or rotation rate of the detector, and σ_{imu}, which is the angular random walk (ARW) of the IMU.

An example screenshot of the input and output results window is shown in Figure 8. The top graph of Figure 8 shows cross-boresight error vs. time. The value starts at t_o with the typical error resulting from the star tracker at each observation. However, this error is slowly reduced using the weighted least squares method until steady state error is achieved. The error shown during the initialization time frame does not show sawtooth effects from the IMU. The bottom graph of Figure 8 shows the steady state error of the system in the same units as the top graph (1σ CI, μrad). The sawtooth effects are created by error growth due to IMU propagation in-between each of the star tracker readings. The maximum value from this sawtooth-graph is listed as the cross-boresight error (μrad) in Figure 8.

IV. Results

The STAcc program results are verified by using input parameters associated with known, published star tracker configurations and then comparing the predicted performance results with published values. Comparison with existing hardware is difficult, as detailed specifications for star trackers are typically not published. In addition, a typical star tracker specification data sheet contains information for single time observations, which does not yield itself to verifying the IMU least squares implementation.

The predicted performance values as calculated by the STAcc program are compared to published performance values for three commercially available star trackers. Sufficient performance characteristics are available for the three selected star tracker hardware, which enables a reasonable performance estimate of the designed tool with a high level of confidence. For cases where the required input parameters are not avail-

Table 1. Published characteristics of commercially available star trackers.[7–9]

Star Tracker	QE [fraction]	Aperture [mm]	Magnitude [m_V]	Exp. Time [sec]	FOV [deg]	Detector Pixels	Slew Rate [deg/sec]	Stars Tracked
HAST	0.35	110	5.5	0.02	9.47	2048	1.0	1
CT-601/602	0.45*	52	6.0	0.10	7.8	512	1.5	1
Astro 15	0.45*	50	6.5	0.25	13.25	1024	0.3	6*

*Assumed values for parameters not available in published data

Table 2. Published vs. STAcc predicted 1-sigma accuracy.[7–9]

Star Tracker	Cross-boresight Accuracy [μrad] [Published]	[Calculated]
HAST	1.75 to 4.54	2.74
CT-601/602	14.55	17.76
Astro 15	4.85	3.15

able, reasonable values are assumed, which conform to physical limitations and optimal design parameters. Hardware specifications for the selected star trackers as obtained from published data sheets, are found in Table 1. The first star tracker for comparison is the high accuracy star tracker (HAST) from Ball Aerospace, which is also one of the most accurate star trackers commercially available today. For our purposes, the HAST is used for comparison, as the majority of HAST hardware characteristics have been published.[9] The second star tracker is the Ball Aerospace CT-601/602, which also has published data for all the required parameters except QE.[7] The final star tracker to be used is the Jena Optronik Astro 15, which has published data for all characteristics except QE and the number of stars tracked.[8] Unknown QE values for the CT-601 and the Astro 15 are assumed to be 0.45, which is typical of newer detectors. The number of stars tracked for the Astro 15 is assumed to be six because the accuracy specified is the overall accuracy as opposed to the per star accuracy and the maximum number of stars the Astro 15 can track is six. It is assumed that the published accuracy for the star tracker would correspond to the best performance, which is associated with using the maximum number of tracked stars in the calculations. For all the star trackers, photon spread information is unpublished and is assumed to be 0.6 pixels, which should produce near-optimum centroiding for center of mass calculations. Although numerous other star trackers exist, performance numbers are not included due to insufficient published information. The predicted star tracker accuracy using the performance specifications listed in Table 1 for each of the selected commercial star trackers is given in Table 2. It is readily seen, that the STAcc program is capable of predicting star tracker performance and is therefore a reasonable software model for star tracker capabilities.

As a representative example, the STAcc program was used to estimate the effects of combining the Astro 15 star tracker with an IMU. The Astro 15 specifications were input into STAcc along with estimates for unknown parameters which included quantum efficiency and the number of stars tracked. In all examples, the Star Tracker number, which indicates the number of co-boresighted star trackers, is set to 1. The Scalable Inertial Reference Unit for Space (SIRU) is selected for this example.[10] The SIRU serves as a representative IMU for the simulation as the hardware exhibits a low angle random walk and has proven flight heritage. As found in published datasheets, the SIRU has only $0.00015\,^\circ/\sqrt{\text{Hr}}$ of random walk.[10] The results from the STAcc program using the representative star tracker parameters and the selected IMU are shown in Figure 8. Note that it takes up to 44 seconds for the error to be significantly reduced according to the top graph, which depicts the cross boresight error as a function of time steps. The maximum expected error from the bottom graph is shown to be $0.42\,\mu$rad.

The results from STAcc should be cautiously applied to high-noise scenarios. The STAcc lookup tables assume a 9×9 pixel size, without background noise (stray photons), shot noise, or dark current effects. The minimum number of electrons captured per time step is 1,000 and limits the expected signal to noise ratio. Outside of 1,000 electrons per time step, the original Liebe lookup tables (Figure 4) apply.

V. Conclusion

The goal of the Star Tracker Accuracy (STAcc) program is to apply well-understood performance criteria and statistical analysis to predict star tracker accuracy. Methods to estimate the cross-boresight error of a star tracker were expanded to incorporate rotation rates and Inertial Measurement Unit (IMU) sensor measurements. Previous methods solved for rotation rate effects differently and did not incorporate IMUs. STAcc is a useful tool for early mission design as it allows the user to explore optimization and trade studies with star tracker and IMU combinations. Additionally, it can predict capabilities of hardware elements that have not been built yet. The existence of performance estimation tools also allows designers to estimate star tracker performance by selecting commercial off-the-shelf components to build their own star tracker, an increasing trend in cubesat applications. The STAcc program is being used to estimate the accuracy of star tracker with inertial measurement unit combinations for the Integrated Radio and Optical (iROC) project. Verification of the program was conducted to compare the results of the analysis with known star tracker configurations. Results matched well for known star tracker configurations. Future work will explore the effects of noise from stray photons, dark current and other sources.

VI. Appendix

Acronyms

ARW	angular random walk
CI	confidence interval
CMOS	complementary metal-oxide-semiconductor
FOV	field of view
HAS2	high accuracy star tracker imaging sensor two
HAS3	high accuracy star tracker imaging sensor three
HAST	high accuracy star tracker
HiRISE	High Resolution Imaging Science Experience
IMU	inertial measurement unit
iROC	Integrated Radio and Optical Communication
LCRD	Low Earth Orbit Communication Relay Demonstration
LLCD	Lunar Laser Communication Demonstration
MRO	Mars Reconnaissance Orbiter
NASA	National Aeronautics and Space Administration
PSF	point spread function
QE	quantum efficiency
RSS	root sum square
SIRU	scalable inertial reference Unit for space
STAcc	Star Tracker Accuracy

References

[1]Raible, D., Romanofsky, R., Budinger, J., Nappier, J., Hylton, A., Swank, A. J., and Nerone, A. L., "On the Physical Realizability of Hybrid RF and Optical Communications Platforms for Deep Space Applications," *32nd Inernational Communications Satellite Systems Conference*, AIAA, San Diego, CA, 2014.

[2]NASA, "NASA Laser Communication System Sets Record with Data Transmission to and from Moon," Oct 2013, [Online; accessed 22-Oct-2014].

[3]Liebe, C. C., "Accuracy performance of star trackers - a tutorial," *Aerospace and Electronic Systems, IEEE Transactions on*, Vol. 38, No. 2, 2002.

[4]Dzamba, T. and Enright, J., "Optical trades for evolving a small arcsecond star tracker," *Aerospace Conference*, IEEE, Big Sky, MT, 2013.

[5]Jia, H., Yang, J., Li, X., Yang, J., Yang, M., Liu, Y., and Hao, Y., "Systematic error analysis and compensation for high accuracy star centroid estimation of star tracker," *Science China Technological Sciences*, Vol. 53, No. 11, 2010.

[6]Borenstein, M., Hedges, L., Higgins, J., and Rothstein, H., *Introduction to Meta-Analysis*, Wiley, New Jersey, 2009.

[7]Ball Aerospace & Technologies Corp., Boulder, CO, *CT-601 High Accuracy Star Tracker*, [Online; accessed 20-Nov-2014].

[8]Jena Optronik GmbH, Jena, Germany, *Autonomous Star Sensor ASTRO 15*, [Online; accessed 20-Nov-2014].

[9]Michaels, D. and Speed, J., "Ball aerospace star tracker achieves high tracking accuracy for a moving star field," *Aerospace Conference*, IEEE, 2005.

[10]Northrop Grumman Systems Corporation, Woodland Hills, CA, *Scalable SIRU*, 2013, [Online; accessed 20-Nov-2014].

[11]Israel, D. J., Edwards, B. L., Wilson, K. E., and Moores, J. D., "An Optical Communications Pathfinder for the Next Generation Tracking and Data Relay Satellite," *13th International Conference on Space Operations*, Pasadena, CA, 2014.

[12]Jørgensen, J., Denver, T., Baurizio, B., and Jørgensen, P., "MicroASC a Miniature Star Tracker, Small Satellites for Earth Observations," *Fourth International Symposium of the International Academy of Astronautics, Berlin*, 2003.